APL Materials

High-throughput screening of perovskite oxynitride and oxide materials for visible-light photocatalysis

Cite as: APL Mater. **6**, 101103 (2018); https://doi.org/10.1063/1.5041784
Submitted: 26 May 2018 . Accepted: 14 September 2018 . Published Online: 01 October 2018

Keisuke Sawada, and Takahito Nakajima

High-throughput screening of perovskite oxynitride and oxide materials for visible-light photocatalysis

Keisuke Sawada and Takahito Nakajima[a]
Computational Molecular Science Research Team, RIKEN Center for Computational Science, 7-1-26 Minatojima-minami, Cyuo-ku, Kobe, Hyogo 650-0047, Japan

(Received 26 May 2018; accepted 14 September 2018; published online 1 October 2018)

We performed a high-throughput screening of 29 160 perovskite oxynitrides and oxides in order to discover novel photocatalysts for water splitting by visible light. Efficient high-throughput simulations with density functional theory were performed on the K computer, which is a massively parallel multi-core supercomputer in Japan. By applying the screening procedure to the entire set of compounds in the database, 42 potential perovskite-photocatalyst candidates for visible-light water splitting were discovered, including 34 newly proposed perovskites. Of the 42 potential candidates, six perovskites, viz., $NaWO_2N$, KWO_2N, $MgWON_2$, $CaVO_2N$, $CaAl_{1/3}W_{2/3}O_2N$, and $CaV_{2/3}Fe_{1/3}O_3$, are desirable in terms of cost.
https://doi.org/10.1063/1.5041784

Water splitting using only sunlight is an artificial photosynthetic reaction that produces H_2 and O_2 gasses. The photocatalytic semiconductor plays a central role in this artificial photosynthetic water-splitting reaction.[1–3] Water splitting on TiO_2 under ultraviolet light was first realized by Fujishima and Honda.[4] Since then, a variety of photocatalytic semiconductors that operate under ultraviolet light have been described; however, few studies on semiconductors that operate under visible light have been reported.[5–7] Photocatalytic-semiconductor materials that absorb at visible-light wavelengths (600–700 nm) are required to effectively utilize the broad solar spectrum.[8]

Perovskite oxides and oxynitrides are extensively studied visible-light driven photocatalysts;[9–12] however, they are currently known to exhibit low photocatalytic performance. Recently, Pan *et al.* reported that $LaMg_xTa_{1-x}O_{1+3x}N_{2-3x}$ ($x \geq 1/3$), which is a solid solution of $LaTaON_2$ and $LaMg_{2/3}Ta_{1/3}O_3$, exhibits water splitting under visible light.[13–15] They also reported that $LaSc_xTa_{1-x}O_{1+2x}N_{2-2x}$ ($x \geq 1/2$) exhibits visible-light water splitting at wavelengths as high as 600 nm.[15] These findings suggest that high visible-light photocatalytic performance can be achieved by mixing different perovskite compounds.

Computational screening techniques are powerful and efficient approaches for the discovery of new water-splitting photocatalysts.[16–20] Herein we report the results of systematic high-throughput computational simulations of perovskite photocatalysts and novel candidates for visible-light water splitting that were discovered using this computational screening technique. In particular, we performed high-throughput, large-scale computational simulations of perovskite photocatalysts using the K computer, which is a massively parallel multi-core supercomputer. Using similar computational screening techniques on the K computer, we recently discovered novel candidates for lead-free perovskite solar cells and proposed 51 low-toxic halide single and double perovskites.[21] In this study, we considered a total of 29 160 perovskite oxides and oxynitrides with the general formula $AB_xB'_{1-x}O_{1+3x}N_{2-3x}$ ($x = 0$, 1/3, and 2/3) that are formed by the mixing of two single perovskites with a common A-site element. The A-site element was chosen from nine cations, viz., Na, K, Rb, Cs, Mg, Ca, Sr, Ba, and La. For the B/B′-site elements, 40 cations were used, viz., Mg, Ca, Sr, Ba,

[a]Electronic mail: nakajima@riken.jp

Sc, Y, Ti, Zr, Hf, V, Nb, Ta, Cr, Mo, W, Mn, Re, Fe, Ru, Os, Co, Rh, Ir, Ni, Pd, Pt, Cu, Ag, Au, Zn, Cd, Hg, Al, Ga, In, Tl, Si, Ge, Sn, and Pb.

Prior to the material screening procedure, the computational results were compiled as a material database. The database is available as an Excel file in the supplementary material. The database was constructed as follows (full details are available in the supplementary material):

1. The overall charge of each compound was checked to ensure that each chemical composition was neutral using typical atomic oxidation states.[22] As a result, 3284 compounds were found to be charge-neutral.
2. For compounds satisfying the charge-neutrality criterion, position and cell optimizations were performed with Gaussian smearing using density functional theory (DFT) calculations based on plane-wave basis sets. Optimizations were performed using the projector-augmented wave (PAW) method[23,24] implemented in the Vienna *Ab Initio* Simulation Package (VASP).[25] We adopted the PBE functional[26] as the exchange–correlation functional in these DFT calculations. To explore the most stable structure during structure optimization, three types of lattice were considered, viz., non-distorted cubic, distorted orthorhombic, and distorted monoclinic structures (Fig. S1 in the supplementary material). The opposite (*trans*) and adjacent (*cis*) configurations of anionic O or N sites were also considered in the unit cells of all lattices.
3. After the most stable structures were obtained, their formation energies, ΔE, were calculated, after which the unstable compounds ($\Delta E \geq 0$) were excluded from subsequent calculations.
4. We determined which systems were metallic and excluded them from subsequent calculations. The structures of the remaining 558 nonmetallic compounds were re-optimized using the PBE functional without smearing.
5. The re-optimized structures were examined in order to determine which were perovskites; this led to 417 perovskite compounds. The structures of these 417 compounds are provided as VASP POSCAR files in the supplementary material.
6. Bandgaps were calculated using the PBE functional with spin–orbit (SO) coupling. We excluded compounds with bandgaps that exceeded 3.1 eV from subsequent calculations, reducing the number of possible compounds from 417 to 328.
7. To determine more accurate bandgaps, we used the hybrid HSE06 functional[27,28] with SO coupling; approximate bandgaps were evaluated by extrapolation[21] because the full SO-HSE06 calculation was too computational-resource demanding. We verified the accuracies of the SO-HSE06 bandgaps by comparison with experimental data, as shown in Fig. S2; corresponding energy values and the systems included in the correlation are listed in Table SI. The mean absolute error among these bandgaps was less than 0.3 eV. The bandgap extrapolation equation is expressed as

$$E_{\mathrm{g}}^{\text{SO-HSE06}}(k) \cong E_{\mathrm{g}}^{\text{SO-PBE}}(k) + E_{\mathrm{g}}^{\text{HSE06},\Gamma}(k_{\mathrm{s}}) - E_{\mathrm{g}}^{\text{PBE},\Gamma}(k_{\mathrm{s}}), \tag{1}$$

   where the first term is the bandgap calculated using the SO-PBE functional with the original k-point sampling ($2 \times 4 \times 4$) and the second and third terms are the direct bandgaps on the Γ point computed using the spin-free HSE06 and PBE functionals with small k-point k_{s} sampling ($1 \times 2 \times 2$), respectively. These bandgaps were calculated from the Kohn–Sham levels in the SCF solutions.
8. The band-edge positions of the valence-band maxima (VBM) and the conduction band minima (CBM) in the remaining 328 semiconductors were evaluated. To determine the positions of the CBMs and VBMs, we used the empirical equation proposed by Butler and Ginley.[29] In this equation, the CBM and VBM are derived from the geometric averages of the absolute electronegativities of neutral atoms and the bandgap. The validity of this equation was confirmed by Xu and Schoonen for multiple metallic oxides.[30] In the present work, the CBM (E_{C}) and VBM (E_{V}) for $\mathrm{AB}_x\mathrm{B'}_{1-x}\mathrm{O}_{1+3x}\mathrm{N}_{2-3x}$ can be represented as

$$E_{\mathrm{C}} = \left[\chi(\mathrm{A})^a \chi(\mathrm{B})^b \chi(\mathrm{B'})^{b'} \chi(\mathrm{O})^o \chi(\mathrm{N})^n\right]^{\frac{1}{a+b+b'+o+n}} - \frac{1}{2}E_{\mathrm{g}}^{\text{SO-HSE06}} + E_0 + E_{\text{shift}}, \tag{2}$$

$$E_V = E_C + E_g^{\text{SO-HSE06}}, \tag{3}$$

where χ(A), χ(B), χ(B′), χ(O), and χ(N) denote the absolute electronegativities of A, B, B′, O, and N atoms, respectively, $E_g^{\text{SO-HSE06}}$ is the bandgap calculated by Eq. (2), and E_0 is the difference between the potential of the SHE and the vacuum level (E_0 = −4.5 eV[31]). The absolute electronegativities were estimated from the arithmetic mean of the first ionization potential and electron affinity.[32] In the present work, the positions of the calculated band edges were shifted by E_{shift} = −0.66, −0.35, and 0.13 eV for $AB_xB'_{1-x}O_{1+3x}N_{2-3x}$ with x = 0, 1/3, and 2/3, respectively, such that the experimental band edges of the CBMs and VBMs of $LaTaON_2$,[15] $CaTaO_2N$,[33] $SrTaO_2N$,[33] $BaTaO_2N$,[33] $NaTaO_3$,[34] and $KTaO_3$[34] were reproduced well. Experimentally, samples are measured on a surface, and the effect of the polarized surface in water is inherently included in the valence and conduction band positions. Therefore, by introducing the E_{shift} extrapolated from experimental studies, we can indirectly include an effect of the polar surfaces on the band-edge positions. To evaluate the band-edge positions from Eqs. (2) and (3), it is assumed that a compound is immersed in water with pH at the point of zero charge (pH_{PZC}) of a material. To estimate the band-edge position with pH different from the PZC, we need to know the pH_{PZC} of each compound. Basically, the pH_{PZC} is measured by experiments and is not easy to theoretically estimate. Thus, while one ideally would take into account the effect of the fact that the different materials have different PZC values on the predicted band-edge position, we neglect this effect here.

9. The hole and electron effective masses were calculated for the 417 compounds using the PBE functional.

Following the previous computational screening procedures for photocatalytic perovskites,[18–20] we set the following criteria to discover perovskite-photocatalyst candidates capable of visible-light water splitting from the database:

1. Compounds that were charge neutral were retained.
2. Compounds that met the formation energy criterion, $\Delta E < 0$ eV/atom, were selected.
3. Compounds with perovskite structures were retained.
4. Compounds with bandgaps between 1.65 and 3.1 eV at the SO-HSE06 level were selected; this range corresponds to the visible region (about 400–750 nm) of the solar spectrum.
5. On the basis of the experimental results, Pan *et al.* suggested that CBMs and VBMs near the threshold potentials for the evolution of H_2 and O_2 gasses are good conditions for water splitting under visible light;[15] the optimal CBM and VBM ranges proposed are −0.6 to −0.5 eV and 1.5–1.6 eV (vs. the standard hydrogen electrode), respectively. In accordance with their proposal, we set the CBM and VBM criteria to −0.6 and 1.5 eV, respectively, and an acceptable computational error of ±0.45 eV was added to these values.
6. In order for the photocatalysts to be environmentally friendly, the inclusion of toxic elements is undesirable. Therefore, we also excluded compounds that contain Cd, Tl, Hg, and Pb.

The hole and electron mobilities, which are evaluated from the hole and electron effective masses, respectively, were not adopted in the present screening procedure because it is not yet known whether the hole and electron mobilities affect the photocatalytic activities. For the same reason, a screening criterion on whether a compound is the direct-gap material or not was not adopted.

The above design criteria identified 42 potential candidates as visible-light-driven water-splitting perovskite photocatalysts; these candidates, the bandgaps, the band-edge positions, and the hole and electron effective masses are listed in Table I. The 42 potential candidates consist of 3 $AB'ON_2$, 30 $AB_{1/3}B'_{2/3}O_2N$, and 9 $AB_{2/3}B'_{1/3}O_3$-type perovskites. Most of the potential candidates are $AB_{1/3}B'_{2/3}O_2N$-type perovskites. The candidates include 34 new compounds as well as eight previously known photoactive compounds, viz., $LaNbON_2$,[35] $LaTaON_2$,[36,37] $CaNbO_2N$,[38] $CaTaO_2N$,[39–41] $SrNbO_2N$,[38,42] $SrTaO_2N$,[40,41] $BaNbO_2N$,[38,43] and $LaTiO_2N$.[44,45] Of the newly identified compounds, $CaNb_{2/3}Fe_{1/3}O_3$[46] and $SrNb_{2/3}Fe_{1/3}O_3$[46,47] have been fabricated experimentally, but their photocatalytic properties related to water splitting have not been investigated. $RbWO_2N$

TABLE I. Potential visible-light-driven water-splitting perovskite-photocatalyst candidates. E_C and E_V are relative to the standard hydrogen electrode.

	System	E_g (eV)	Gap type	E_C (eV)	E_V (eV)	m_e (m_0)	m_h (m_0)
$AB'ON_2$ ($x = 0$)	$MgWON_2$	1.91	Indirect	−0.30	1.61	−0.89	1.63
	$LaNbON_2$	2.08	Indirect	−0.74	1.34	−0.64	2.28
	$LaTaON_2$	2.15	Indirect	−0.74	1.42	−0.36	0.51
$AB_{1/3}B'_{2/3}O_2N$ ($x = 1/3$)	$NaMoO_2N$	1.86	Direct	−0.37	1.49	−0.50	2.23
	$NaWO_2N$	1.69	Indirect	−0.16	1.53	−0.38	2.42
	$KMoO_2N$	1.87	Indirect	−0.55	1.32	−0.54	1.76
	KWO_2N	1.66	Direct	−0.32	1.34	−0.41	1.83
	$RbWO_2N$	1.99	Indirect	−0.52	1.46	−0.47	1.79
	$CaSc_{1/3}W_{2/3}O_2N$	2.10	Direct	−0.76	1.34	−1.61	32.8
	$CaVO_2N$	1.94	Direct	−0.79	1.15	−0.74	2.28
	$CaV_{1/3}Nb_{2/3}O_2N$	2.10	Indirect	−0.81	1.29	−1.51	15.1
	$CaV_{1/3}Ta_{2/3}O_2N$	2.02	Indirect	−0.74	1.27	−1.20	5.23
	$CaNb_{1/3}V_{2/3}O_2N$	2.04	Indirect	−0.81	1.23	−1.21	23.6
	$CaNbO_2N$	2.30	Indirect	−0.88	1.42	−0.70	1.21
	$CaNb_{1/3}Ta_{2/3}O_2N$	2.61	Indirect	−1.00	1.60	−0.85	10.8
	$CaTa_{1/3}Nb_{2/3}O_2N$	2.63	Indirect	−1.03	1.60	−0.86	14.7
	$CaTaO_2N$	2.62	Direct	−1.00	1.62	−0.76	4.05
	$CaCo_{1/3}W_{2/3}O_2N$	1.72	Indirect	−0.49	1.23	−2.05	5.84
	$CaAl_{1/3}W_{2/3}O_2N$	1.84	Direct	−0.64	1.20	−1.99	8.05
	$CaGa_{1/3}W_{2/3}O_2N$	2.13	Indirect	−0.80	1.33	−2.31	17.9
	$CaIn_{1/3}W_{2/3}O_2N$	2.33	Indirect	−0.91	1.42	−2.36	30.0
	$SrY_{1/3}W_{2/3}O_2N$	2.20	Indirect	−0.90	1.30	−1.12	6.15
	$SrNbO_2N$	2.20	Direct	−0.90	1.30	−0.49	1.95
	$SrNb_{1/3}Ta_{2/3}O_2N$	1.69	Indirect	−0.62	1.07	−0.56	0.62
	$SrTa_{1/3}Nb_{2/3}O_2N$	2.13	Indirect	−0.85	1.28	−0.58	2.25
	$SrTaO_2N$	2.04	Indirect	−0.78	1.26	−0.56	1.35
	$SrGa_{1/3}W_{2/3}O_2N$	1.73	Direct	−0.67	1.06	−1.48	2.37
	$BaNbO_2N$	1.99	Direct	−0.63	1.36	−0.50	1.22
	$BaTa_{1/3}Nb_{2/3}O_2N$	1.79	Direct	−0.52	1.27	−0.50	1.40
	$BaIn_{1/3}W_{2/3}O_2N$	1.73	Direct	−0.52	1.22	−1.35	1.71
	$LaTiO_2N$	2.39	Direct	−0.70	1.69	−1.10	2.74
	$LaW_{1/3}Sc_{2/3}O_2N$	2.49	Direct	−0.69	1.81	−1.85	6.65
	$LaW_{1/3}Al_{2/3}O_2N$	2.23	Indirect	−0.58	1.65	−2.53	4.06
$AB_{2/3}B'_{1/3}O_3$ ($x = 2/3$)	$CaV_{2/3}Fe_{1/3}O_3$	1.94	Indirect	−0.24	1.70	−2.16	3.82
	$CaNb_{2/3}Fe_{1/3}O_3$	1.94	Indirect	−0.18	1.76	−1.79	7.02
	$CaNb_{2/3}Pd_{1/3}O_3$	2.12	Indirect	−0.23	1.89	−1.50	4.14
	$SrNb_{2/3}Fe_{1/3}O_3$	1.92	Indirect	−0.24	1.68	−3.55	3.28
	$SrNb_{2/3}Pd_{1/3}O_3$	2.16	Indirect	−0.33	1.83	−1.17	4.09
	$SrTa_{2/3}Fe_{1/3}O_3$	2.36	Indirect	−0.44	1.93	−1.52	4.46
	$SrTa_{2/3}Pd_{1/3}O_3$	2.27	Indirect	−0.35	1.91	−1.35	4.75
	$SrAl_{2/3}Mo_{1/3}O_3$	2.46	Indirect	−0.66	1.80	−1.77	2.77
	$SrSn_{2/3}W_{1/3}O_3$	2.09	Indirect	−0.24	1.85	−3.78	1.60

has not been synthesized, but its structural and electronic properties have been investigated by DFT calculations.[48]

Our computational screening did not identify $LaMg_{1/3}Ta_{2/3}O_2N$, which has been reported to be a promising material for water splitting under visible light.[13–15] The rejection of $LaMg_{1/3}Ta_{2/3}O_2N$ is a consequence of its bandgap being significantly overestimated (Table SI). To clarify why the calculated bandgap for $LaMg_{1/3}Ta_{2/3}O_2N$ was significantly larger than the experimental value, we investigated the relationship between the location of Mg in its structure and the bandgap. In addition to the disordered Mg configuration used in the present work, we prepared two other types of unit cells with differently distributed Mg sites, namely, Mg-plane-ordered and Mg-chain-ordered configurations, as shown in Figure S3. The bandgaps for these structures were calculated to be 3.02, 2.04, and 1.25 eV, respectively. The bandgaps were observed to vary dramatically with the Mg-site location. The bandgap calculated for the Mg-plane-ordered structure is consistent with the experimental bandgap (2.08 eV),

whereas that of the Mg-disordered structure is too large when compared with the experimental result. Consequently, $LaMg_{1/3}Ta_{2/3}O_2N$ was inadvertently excluded during the band-edge screening process. We speculatively attribute the lower experimental bandgap to Mg-atom clustering during the formation of the solid solution. Moreover, for some potential candidates shown in Table I, we investigated the dependency of the arrangement of B- (B′-) and X-site elements on the bandgaps. We found that the bandgaps drastically change with the ordering of B- (B′-) and X-site elements as well as the case of $LaMg_{1/3}Ta_{2/3}O_2N$. The details are shown in the supplementary material.

Figure 1 displays the band-edge positions of the 42 potential candidates. We found that the $AB_{2/3}B'_{1/3}O_3$-type perovskites tend to have higher VBMs than the $AB'ON_2$- and $AB_{1/3}B'_{2/3}O_2N$-type perovskites. The VBM of an $AB_{2/3}B'_{1/3}O_3$-type perovskite is constructed mainly from the d orbitals of the B and B′ elements and the p orbitals of the oxygen, while those of the $AB'ON_2$- and $AB_{1/3}B'_{2/3}O_2N$-type perovskites are mainly constructed from the p orbitals of the nitrogen (Figs. S4–S9) that lower the VBM. This trend of the VBM in oxide and oxynitride perovskites is consistent with that which was previously reported.[49] Similarly, the CBM of an $AB_{2/3}B'_{1/3}O_3$-type perovskite is higher than those of the $AB'ON_2$- and $AB_{1/3}B'_{2/3}O_2N$-type perovskites. The CBM of an $AB_{2/3}B'_{1/3}O_3$-type perovskite is mainly constructed from the d orbitals of the B and B′ elements and the p orbitals of the oxygen, while the CBMs of $AB'ON_2$- and $AB_{1/3}B'_{2/3}O_2N$-type perovskites are predominantly constructed from the d orbitals of the B or B′ atoms. This suggests that the mixing of B/B′-d orbitals and the p orbitals of the oxygen in the $AB_{2/3}B'_{1/3}O_3$-type perovskite results in higher CBMs.

Among the 42 potential candidates, 33 compounds adopt d^0 or d^{10} electronic configurations. We found that the oxynitride candidates mainly possess d^0/d^{10} electronic configurations.

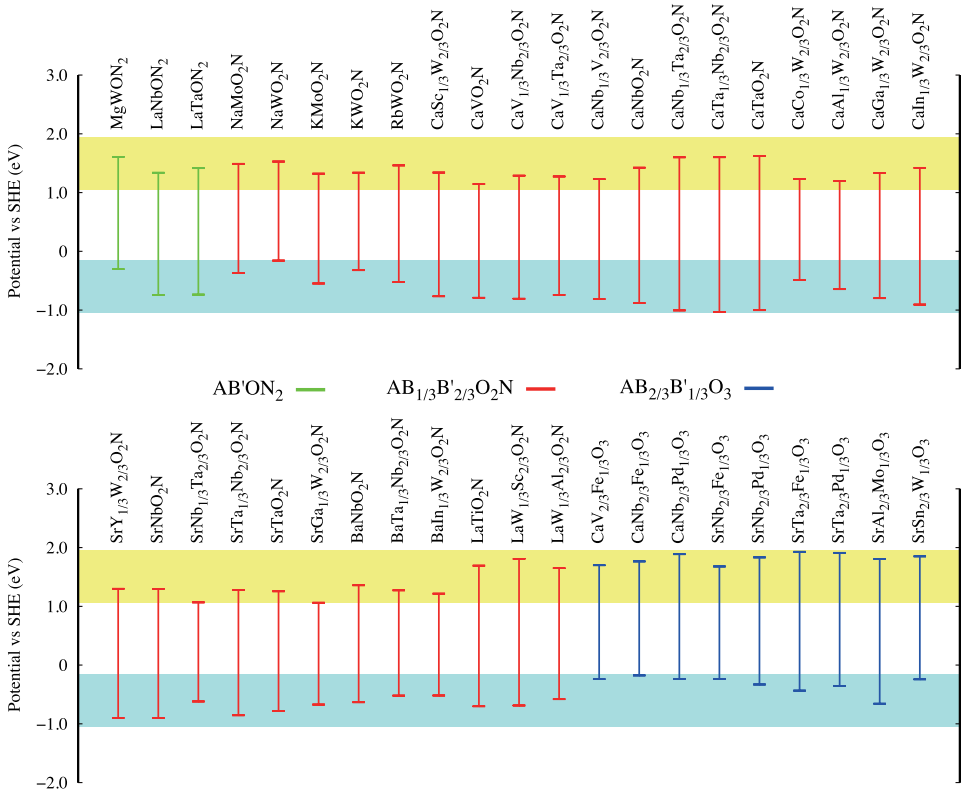

FIG. 1. Band-edge positions of potential $AB_xB'_{1-x}O_{1+3x}N_{2-3x}$ (x = 0, 1/3, and 2/3) perovskite candidates. Green, red, and blue bars correspond to compounds with $AB'ON_2$, $AB_{1/3}B'_{2/3}O_2N$, and $AB_{2/3}B'_{1/3}O_3$ structures, respectively. The light blue and yellow regions highlight the acceptable conduction-band-minima (−1.05 to −0.15 eV) and valence-band-maxima (1.05–1.95 eV) adopted in the present work, respectively. Band-edge positions are relative to the standard hydrogen electrode (SHE).

Other nine compounds have partially occupied d levels, viz., $CaCo_{1/3}W_{2/3}O_2N$ (d^6), $CaV_{2/3}Fe_{1/3}O_3$ (d^6), $CaNb_{2/3}Fe_{1/3}O_3$ (d^6), $CaNb_{2/3}Pd_{1/3}O_3$ (d^8), $SrNb_{2/3}Fe_{1/3}O_3$ (d^6), $SrNb_{2/3}Pd_{1/3}O_3$ (d^8), $SrTa_{2/3}Fe_{1/3}O_3$ (d^6), $SrTa_{2/3}Pd_{1/3}O_3$ (d^8), and $SrSn_{2/3}W_{1/3}O_3$ (d^2). Most of the candidates with partially occupied d levels are perovskite oxides. Table I also reveals that eight potential $AB_{2/3}B'_{1/3}O_3$-type perovskite candidates have partially occupied d electronic configurations, except for $SrAl_{2/3}Mo_{1/3}O_3$. Hence, we expect that visible-light driven water splitting is realized by the mixing of metallic ions with partially occupied d levels in perovskite oxides. This finding is supported by experimental reports; the incorporation of partially occupied d transition metal cations into these oxides has been shown to result in water splitting under visible light.[7,50,51] Consequently, we suggest that perovskite oxynitrides with d^0/d^{10} electronic configurations, or perovskite oxides with partially occupied d orbitals, are desirable as visible-light-driven water-splitting photocatalysts with adequate bandgaps and band edge positions.

It is also important to exclude rare and expensive elements from these candidate materials. Most of the existing perovskite photocatalysts contain rare metals such as Ta and La. To avoid issues associated with production costs, the replacement of rare metals with inexpensive and abundant elements, such as 3d transition metals, is required.[52] By selecting perovskites from the 42 potential candidates containing elements less expensive than vanadium,[53] six compounds, viz., $NaWO_2N$, KWO_2N, $MgWON_2$, $CaVO_2N$, $CaAl_{1/3}W_{2/3}O_2N$, and $CaV_{2/3}Fe_{1/3}O_3$, were selected. While these six perovskites have not yet been synthesized, we expect that $CaVO_2N$ and $CaV_{2/3}Fe_{1/3}O_3$ are synthetically viable because $CaNbO_2N$ and $CaNb_{2/3}Fe_{1/3}O_3$, which contain B-site elements from the same group, have already been synthesized.

Finally, we discuss the comparison with previous computational screenings based on the DFT.[16,18–20,54] The search space of our screening consists of 29 160 compounds. Wu *et al.*[16] conducted a computational screening for 2948 compounds to discover promising water-splitting photocatalysts. Castelli *et al.*[18–20] investigated up to 19 000 perovskite compounds. Yan *et al.*[54] performed hybrid screening of computational and experimental methods for 174 oxides with structure motif VO_4 extracted from the Materials Project database. To the best of our knowledge, our investigating space is the largest in the computational screening studies of photocatalytic perovskites. For the composition of the perovskite, we consider two types of B-site cations to construct mixed perovskite structures, whereas the previous studies considered only one type of B-site cation. Therefore, a large number of unknown mixed perovskites are investigated in our screening. For the estimation of the band-edge positions, we and Castelli *et al.* employed the empirical method,[29,30] whereas Wu *et al.* and Yan *et al.* evaluated the band edges from surface slab calculations.[55–57] The effect of surface polarity and termination is an important factor for the band alignment in perovskite materials.[58,59] Although the band-edge positions determined by the slab calculations involves the polar and termination effect on the surface,[60] the slab calculations require expensive computational costs. In our system, which includes 60 atoms in the unit cell, since much larger computational efforts were required to perform the slab calculations, we adopted the empirical method combined with the energy shift [Eqs. (2) and (3)].

To summarize, we computationally screened perovskite oxynitrides and oxides in order to discover novel photocatalysts for water splitting under visible light. The exploration space extended to 29 160 compounds. To achieve efficient high-throughput computations on this large number of candidate compounds, we took advantage of the K computer. The computational results for all of the $AB_xB'_{1-x}O_{1+3x}N_{2-3x}$ (x = 0, 1/3, and 2/3) compounds were compiled into a materials database. By setting criteria for formation energies, bandgaps, and band-edge positions, 42 potential candidate perovskite photocatalysts for visible-light water splitting were obtained. Among them, eight compounds were already known to be water-splitting materials, confirming the validity of our computational-screening approach. The remaining 34 perovskites were newly discovered as potential catalysts in this work. Of the 42 potential candidates, six particular perovskites, viz., $NaWO_2N$, KWO_2N, $MgWON_2$, $CaVO_2N$, $CaAl_{1/3}W_{2/3}O_2N$, and $CaV_{2/3}Fe_{1/3}O_3$, are desirable in terms of cost effectiveness. We anticipate that the perovskite materials proposed in this work will be synthesized and characterized for their water-splitting properties under visible light in the future.

See supplementary material for details of computational methods, screening procedures, and tables of data for the candidate perovskites (PDF); computational materials database (XLSX); and VASP POSCAR files of the optimized structures of 417 compounds (TXT).

This work was supported by the Next-Generation Supercomputer project (the K computer project) and FLAGSHIP2020 within priority study 5 (Development of new fundamental technologies for high-efficiency energy creation, conversion/storage and use) of MEXT, Japan, and the FOCUS Establishing Supercomputing Center of Excellence.

[1] A. J. Bard and M. A. Fox, Acc. Chem. Res. **28**, 141 (1995).
[2] H. Zhou, X. F. Li, T. X. Fan, F. E. Osterloh, J. Ding, E. M. Sabio, D. Zhang, and Q. X. Guo, Adv. Mater. **22**, 951 (2010).
[3] B. A. Pinaud, J. D. Benck, L. C. Seitz, A. J. Forman, Z. Chen, T. G. Deutsch, B. D. James, K. N. Baum, G. N. Baum, S. Ardo, H. Wang, E. Miller, and T. F. Jaramillo, Energy Environ. Sci. **6**, 1983 (2013).
[4] A. Fujishima and K. Honda, Nature **238**, 37 (1972).
[5] A. Kudo and Y. Miseki, Chem. Soc. Rev. **38**, 253 (2009).
[6] T. Hisatomi, J. Kubota, and K. Domen, Chem. Soc. Rev. **43**, 7520 (2014).
[7] R. Asai, H. Nemoto, Q. Jia, K. Saito, A. Iwase, and A. Kudo, Chem. Commun. **50**, 2543 (2014).
[8] K. Maeda and K. Domen, J. Phys. Chem. Lett. **1**, 2655 (2010).
[9] P. Kanhere and Z. Chen, Molecules **19**, 19995 (2014).
[10] W. Wang, M. O. Tadé, and Z. Shao, Chem. Soc. Rev. **44**, 5371 (2015).
[11] G. Zhang, G. Liu, L. Z. Wang, and J. T. S. Irvine, Chem. Soc. Rev. **45**, 5951 (2016).
[12] M. Ahmed and G. Xinxin, Inorg. Chem. Front. **3**, 578 (2016).
[13] C. Pan, T. Takata, M. Nakabayashi, T. Matsumoto, N. Shibata, Y. Ikuhara, and K. Domen, Angew. Chem., Int. Ed. **54**, 2955 (2015).
[14] C. Pan, T. Takata, and K. Domen, Chem. Eur. J. **22**, 1854 (2016).
[15] C. Pan, T. Takata, K. Kumamoto, S. S. K. Ma, K. Ueda, T. Minegishi, M. Nakabayashi, T. Matsumoto, N. Shibata, Y. Ikuhara, and K. Domen, J. Mater. Chem. A **4**, 4544 (2016).
[16] Y. Wu, P. Lazic, G. Hautier, K. Persson, and G. Ceder, Energy Environ. Sci. **6**, 157 (2013).
[17] A. K. Singh, K. Mathew, H. L. Zhuang, and R. G. Hennig, J. Phys. Chem. Lett. **6**, 1087 (2015).
[18] I. E. Castelli, T. Olsen, S. Datta, D. D. Landis, S. Dahl, K. S. Thygesen, and K. W. Jacobsen, Energy Environ. Sci. **5**, 5814 (2012).
[19] I. E. Castelli, D. D. Landis, K. S. Thygesen, S. Dahl, I. Chorkendorff, T. F. Jaramillo, and K. W. Jacobsen, Energy Environ. Sci. **5**, 9034 (2012).
[20] I. E. Castelli, J. M. Garca-Lastra, F. Hüser, K. S. Thygesen, and K. W. Jacobsen, New J. Phys. **15**, 105026 (2013).
[21] T. Nakajima and K. Sawada, J. Phys. Chem. Lett. **8**, 4826 (2017).
[22] N. N. Greenwood and A. Earnshow, *Chemistry of the Elements*, 2nd ed. (Butterworth–Heinemann, UK, 1997).
[23] P. E. Blöchl, Phys. Rev. B **50**, 17953 (1994).
[24] G. Kresse and D. Joubert, Phys. Rev. B **59**, 1758 (1999).
[25] G. Kresse and J. Furthmüller, Comput. Mater. Sci. **6**, 15 (1996).
[26] J. P. Perdew, K. Burke, and M. Ernzerhof, Phys. Rev. Lett. **77**, 3865 (1996).
[27] J. Heyd, G. E. Scuseria, and M. Ernzerhof, J. Chem. Phys. **118**, 8207 (2003).
[28] A. Krukau, O. Vydrov, A. Izmaylov, and G. Scuseria, J. Chem. Phys. **125**, 224106 (2006).
[29] M. A. Butler and D. S. Ginley, J. Electrochem. Soc. **125**, 228 (1978).
[30] Y. Xu and M. A. A. Schoonen, Am. Mineral. **85**, 543 (2000).
[31] J. O. M. Bockris and S. U. M. Khan, *Surface Electrochemistry* (Plenum Press, 1993), p. 1014.
[32] R. G. Pearson, Inorg. Chem. **27**, 734 (1988).
[33] S. Balaz, S. H. Porter, P. M. Woodward, and L. J. Brillson, Chem. Mater. **25**, 3337 (2013).
[34] H. Kato and A. Kudo, J. Phys. Chem. B **105**, 4285 (2001).
[35] C. Izawa, T. Kobayashi, K. Kishida, and T. Watanabe, Adv. Mater. Sci. Eng. **2014**, 465720.
[36] L. Meiying, Y. Wansheng, L. Zhibin, T. Takata, K. Domen, and L. Can, Chin. J. Catal. **27**, 556 (2006).
[37] M. Hojamberdiev, M. F. Bekheet, J. N. Hart, J. J. M. Vequizo, A. Yamakata, K. Yubuta, A. Gurlo, M. Hasegawa, K. Domen, and K. Teshima, Phys. Chem. Chem. Phys. **19**, 22210 (2017).
[38] B. Siritanaratkul, K. Maeda, T. Hisatomi, and K. Domen, ChemSusChem **4**, 74 (2011).
[39] J. Xu, C. Pan, T. Takata, and K. Domen, Chem. Commun. **51**, 7191 (2015).
[40] M. Higashi, R. Abe, K. Teramura, T. Takata, B. Ohtani, and K. Domen, Chem. Phys. Lett. **452**, 120 (2008).
[41] M. Higashi, R. Abe, T. Takata, and K. Domen, Chem. Mater. **21**, 1543 (2009).
[42] K. Maeda, M. Higashi, B. Siritanaratkul, R. Abe, and K. Domen, J. Am. Chem. Soc. **133**, 12334 (2011).
[43] T. Hisatomi, C. Katayama, Y. Moriya, T. Minegishi, M. Katayama, H. Nishiyama, T. Yamada, and K. Domen, Energy Environ. Sci. **6**, 3595 (2013).
[44] A. Kasahara, K. Nukumizu, G. Hitoki, T. Takata, J. N. Kondo, M. Hara, H. Kobayashi, and K. Domen, J. Phys. Chem. A **106**, 6750 (2002).
[45] A. Kasahara, K. Nukumizu, T. Takata, J. N. Kondo, M. Hara, H. Kobayashi, and K. Domen, J. Phys. Chem. B **107**, 791 (2003).
[46] T. Nakagawa and S. Nomura, J. Phys. Soc. Jpn. **29**, 1395 (1970).
[47] F. Galasso and J. Pyle, J. Phys. Chem. **67**, 1561 (1963).
[48] E. Orisakwe, R. Marchal, B. Fontaine, R. Gautier, and J.-F. Halet, J. Ceram. Soc. Jpn. **124**, 1056 (2016).
[49] K. Maeda and K. Domen, J. Phys. Chem. C **111**, 7851 (2007).

[50] R. Konta, T. Ishii, H. Kato, and A. Kudo, J. Phys. Chem. B **108**, 8992 (2004).
[51] Y. Sasaki, H. Nemoto, K. Saito, and A. Kudo, J. Phys. Chem. C **113**, 17536 (2009).
[52] S. Chen, T. Takata, and K. Domen, Nat. Rev. Mater. **2**, 17050 (2017).
[53] R. Jaffe, J. Price, M. Hitzman, and F. Slakey, Energy Critical Elements, 2011, see https://www.aps.org/units/fps/newsletters/201107/jaffe.cfm.
[54] Q. Yan, J. Yu, S. K. Suram, L. Zhou, A. Shinde, P. F. Newhouse, W. Chen, G. Li, K. A. Persson, J. M. Gregoire, and J. B. Neaton, Proc. Natl. Acad. Sci. U. S. A. **114**, 3040 (2017).
[55] Y. Wu, M. K. Y. Chan, and G. Ceder, Phys. Rev. B **83**, 235301 (2011).
[56] P. G. Moses, M. Miao, Q. Yan, and C. G. Van de Walle, J. Chem. Phys. **134**, 084703 (2011).
[57] V. Stevanović, S. Lany, D. S. Ginley, W. Tumas, and A. Zunger, Phys. Chem. Chem. Phys. **16**, 3706 (2014).
[58] J. Goniakowski, F. Finocchi, and C. Noguera, Rep. Prog. Phys. **71**, 016501 (2008).
[59] A. Belabbes, J. Furthmüller, and F. Bechstedt, Phys. Rev. B **84**, 205304 (2011).
[60] Y. Hinuma, A. Grüneis, G. Kresse, and F. Oba, Phys. Rev. B **90**, 155405 (2014).